arXiv:1611.07162v1 [astro-ph.SR] 22 Nov 2016

Evidence from stable isotopes and ^{10}Be for solar system formation triggered by a low-mass supernova

Projjwal Banerjee

School of Physics and Astronomy, University of Minnesota, Minneapolis, Minnesota 55455, USA

Yong-Zhong Qian*†

School of Physics and Astronomy, University of Minnesota, Minneapolis, Minnesota 55455, USA; qian@physics.umn.edu

Alexander Heger†

Monash Centre for Astrophysics, School of Physics and Astronomy, Monash University, Victoria 3800, Australia

W. C. Haxton

Department of Physics, University of California, and Lawrence Berkeley National Laboratory, Berkeley, California 94720, USA

About 4.6 billion years ago, some event disturbed a cloud of gas and dust, triggering the gravitational collapse that led to the formation of the solar system. A core-collapse supernova, whose shock wave is capable of compressing such a cloud, is an obvious candidate for the initiating event. This hypothesis can be tested because supernovae also produce telltale patterns of short-lived radionuclides, which would be preserved today as isotopic anomalies. Previous studies of the forensic evidence have been inconclusive, finding a pattern of isotopes differing from that produced in conventional supernova models. Here we argue that these difficulties either do not arise or are mitigated if the initiating supernova was a special type, low in mass and explosion energy. Key to our conclusion is the demonstration that short-lived ^{10}Be can be readily synthesized in such supernovae by neutrino interactions, while anomalies in stable isotopes are suppressed.

* Corresponding author.

† Visiting Professor, Center for Nuclear Astrophysics, Department of Physics and Astronomy, Shanghai Jiao Tong University, Shanghai 200240, China.

Nearly four decades ago Cameron and Truran [1] suggested that the formation of our solar system (SS) might have been due to a single core-collapse supernova (CCSN) whose shock wave triggered the collapse of a nearby interstellar cloud. They recognized that forensic evidence of such an event would be found in CCSN-associated short-lived ($\lesssim 10$ Myr) radionuclides (SLRs) that would decay, but leave a record of their existence in isotopic anomalies. Their suggestion was in fact stimulated by observed meteoritic excesses in ^{26}Mg [2], the daughter of the extinct SLR ^{26}Al with a lifetime of $\tau \sim 1$ Myr. The inferred value of ^{26}Al/^{27}Al in the early SS, orders of magnitude higher than the Galactic background, requires a special source [3].

While simulations support the thesis that a CCSN shock wave can trigger SS formation and inject SLRs into the early SS [4–6], detailed modeling of CCSN nucleosynthesis and an accumulation of data on extinct radionuclides have led to a confusing and conflicting picture [3, 7]. CCSNe of $\gtrsim 15$ solar masses ($M_\odot$) are a major source of stable isotopes such as ^{24}Mg, ^{28}Si, and ^{40}Ca. The contributions from a single CCSN in this mass range combined with the dilution factor indicated by simulations [4–6] would have caused large shifts in ratios of stable isotopes that are not observed [3]. A second problem concerns the relative production of key SLRs: such a CCSN source grossly overproduces ^{53}Mn and ^{60}Fe [3], while producing (relatively) far too little of ^{10}Be. Although the overproduction of ^{53}Mn and ^{60}Fe can plausibly be mitigated by the fallback of inner CCSN material, preventing the ejection of these two SLRs [7, 8], the required fallback must be extremely efficient in high-mass CCSNe.

Here we show that the above difficulties with the CCSN trigger hypothesis can be removed or mitigated, if the CCSN mass was $\lesssim 12\,M_\odot$. The structure of a low-mass CCSN progenitor differs drastically from that of higher-mass counterparts, being compact with much thinner processed shells. Given the CCSN trigger hypothesis, we argue that the stable isotopes alone demand such a progenitor. But in addition, this assumption addresses several other problems noted above. First, we show the yields of ^{53}Mn and ^{60}Fe are reduced by an order of magnitude or more in low-mass CCSNe, making the fallback required to bring the yields into agreement with the data much more plausible. Second, we show that the mechanism by which CCSNe produce ^{10}Be, the neutrino spallation process $^{12}\mathrm{C}(\nu, \nu' pp)^{10}\mathrm{Be}$, differs from other SLR production mechanisms in that the yield of ^{10}Be remains high as the progenitor mass is decreased. Consequently we find that an $11.8\,M_\odot$ model can produce the bulk of the

^{10}Be inventory in the early SS without overproducing other SLRs. We conclude that among possible CCSN triggers, a low-mass one is demanded by the data on both stable isotopes and SLRs.

It has been commonly thought that ^{10}Be is not associated with stellar sources, originating instead only from spallation of carbon and oxygen in the interstellar medium (ISM) by cosmic rays (CRs; e.g., [9]) or irradiation of the early SS material by solar energetic particles (SEPs; e.g., [10, 11]) associated with activities of the proto-Sun. It was noted in Ref. [12] that ^{10}Be can be produced by neutrino interactions in CCSNe, but the result was presented for a single model and no connection to meteoritic data was made. Further, that work adopted an old rate for the destruction reaction $^{10}\mathrm{Be}(\alpha, n)^{13}\mathrm{C}$ that is orders of magnitude larger than currently recommended [13], and therefore, greatly underestimated the ^{10}Be yield.

^{10}Be has been observed in the form of a ^{10}B excess in a range of meteoritic samples. Significant variations across the samples suggest that multiple sources might have contributed to its inventory in the early SS [14–19]. Calcium-aluminum-rich inclusions (CAIs) with $^{26}\mathrm{Al}/^{27}\mathrm{Al}$ close to the canonical value were found to have significantly higher $^{10}\mathrm{Be}/^{9}\mathrm{Be}$ than CAIs with Fractionation and Unidentified Nuclear isotope effects (FUN-CAIs), which also have $^{26}\mathrm{Al}/^{27}\mathrm{Al}$ much less than the canonical value [18]. As FUN-CAIs are thought to have formed earlier than canonical CAIs, it has been suggested [18] that the protosolar cloud was seeded with $^{10}\mathrm{Be}/^{9}\mathrm{Be} \sim 3 \times 10^{-4}$, the level observed in FUN-CAIs, by e.g., trapping Galactic CRs [9], and that the significantly higher $^{10}\mathrm{Be}/^{9}\mathrm{Be}$ values in canonical CAIs were produced later by SEPs [10, 11].

A recent study [20] showed that trapping Galactic CRs led to little ^{10}Be enrichment of the protosolar cloud and long-term production by Galactic CRs could only provide $^{10}\mathrm{Be}/^{9}\mathrm{Be} \lesssim 1.3 \times 10^{-4}$. Instead, CRs from either a large number of CCSNe or a single special CCSN were proposed to account for $^{10}\mathrm{Be}/^{9}\mathrm{Be} \sim 3 \times 10^{-4}$. While this pre-enrichment scenario is plausible, it depends on many details of CCSN remnant evolution and CR production and interaction. Similarly, further production of ^{10}Be by SEPs must have occurred at some level, but the actual contributions are sensitive to the composition, spectra, and irradiation history of SEPs as well as the composition of the irradiated gas and solids [10, 11, 21], all of which are rather uncertain. In view of both the data and uncertainties in CR and SEP models, we consider it reasonable that a low-mass CCSN provided the bulk of the ^{10}Be inventory in the early SS while still allowing significant contributions from CRs and SEPs. Specifically,

we find that such a CCSN can account for ^{10}Be/^{9}Be $= (7.5 \pm 2.5) \times 10^{-4}$ typical of the canonical CAIs [22]. Following the presentation of our detailed results, we will discuss an overall scenario to account for ^{10}Be and other SLRs based on our proposed low-mass CCSN trigger and other sources.

Results

Explosion Modeling

We have calculated CCSN nucleosynthesis for solar-composition progenitors in the mass range of 11.8 to 30 $M_\odot$. Each star was evolved to core collapse, using the most recent version of the 1D hydrodynamic code KEPLER [23, 24]. The subsequent explosion was simulated by driving a piston from the base of the oxygen shell into the collapsing progenitor. Piston velocities were selected to produce explosion energies of 0.1, 0.3, 0.6, and 1.2 B (1 B $= 10^{51}$ ergs) for the 11.8–12, 14, 16, and 18–30 $M_\odot$ models, respectively, to match results from recent CCSN simulations [25, 26]. The material inside the initial radius of the piston was allowed to fall immediately onto the protoneutron star forming at the core. In our initial calculations, shown in Fig. 1 and labeled Case 1 in Table 1, we assume all material outside the piston is ejected. Neutrino emission was modeled by assuming Fermi-Dirac spectra with chemical potentials $\mu = 0$, fixed temperatures $T_{\nu_e} \sim 3$ MeV and $T_{\bar{\nu}_e} \sim T_{\nu_\mu} \sim T_{\nu_\tau} \sim T_{\bar{\nu}_\mu} \sim T_{\bar{\nu}_\tau} \sim 5$ MeV, and luminosities decreasing exponentially from an initial value of 16.7 B s^{-1} per species, governed by a time constant of ~ 3 s. This treatment is consistent with detailed neutrino transport calculations [27] as well as supernova 1987A observations [28]. A full reaction network was used to track changes in composition during the evolution and explosion of each star, including neutrino rates taken from Ref. [29].

Nucleosynthesis Yields

Figure 1 shows the yields normalized to the 11.8 $M_\odot$ model as functions of the progenitor mass for stable isotopes ^{12}C, ^{16}O, ^{24}Mg, ^{28}Si, ^{40}Ca, and ^{56}Fe as well as SLRs ^{10}Be, ^{41}Ca, ^{53}Mn, ^{60}Fe, and ^{107}Pd. It can be seen that except for ^{10}Be, the yields of all other isotopes increase sharply for CCSNe of 14–30 $M_\odot$. Therefore, a high-mass CCSN trigger is problematic, generating unacceptably large shifts in ratios of stable isotopes and overproducing SLRs such as ^{53}Mn and ^{60}Fe [3]. Fallback of $\gtrsim 1\, M_\odot$ of inner material in such CCSNe was

invoked in Ref. [8] to account for the data on the SLRs ^{26}Al, ^{41}Ca, ^{53}Mn, and ^{60}Fe. Using our models (see Supplementary Table 1), we find that similar fallback scenarios and dilution factors are required but the problem with stable isotopes persists (see Supplementary Discussion). In contrast, even for Case 1 without fallback, the yields of the 11.8 $M_\odot$ model (see Supplementary Tables 2 and 3) are consistent with meteoritic constraints for all major stable isotopes (see Supplementary Discussion). We focus on the production of SLRs by this model below.

Figure 1 shows that in contrast to other isotopes, the ^{10}Be yield from ^{12}C via $^{12}\mathrm{C}(\nu,\nu' pp)^{10}\mathrm{Be}$ is relatively insensitive to progenitor mass. This reflects the compensating effects of higher C-zone masses but lower neutrino fluxes (larger C-zone radii) in more massive stars (see Supplementary Discussion for more on SLR production). Our demonstration here that ^{10}Be is a ubiquitous CCSN product of neutrino-induced nucleosynthesis consequently allows us to attribute this SLR to a low-mass CCSN, explaining its abundance level in canonical CAIs, while achieving overall consistency with the data on other SLRs coproduced by other mechanisms in the CCSN. More quantitatively, let R denote a given SLR, I its stable reference isotope, Y_R the total mass yield of R from the CCSN, and f the fraction of the yield that was incorporated into each $M_\odot$ of the protosolar cloud (i.e., the dilution factor). The number ratio of R to I in the early SS due to this CCSN is

$$\left(\frac{N_\mathrm{R}}{N_\mathrm{I}}\right)_\mathrm{ESS} \sim \frac{fY_\mathrm{R}/A_\mathrm{R}}{X_\mathrm{I}^\odot M_\odot/A_\mathrm{I}} \exp\left(-\frac{\Delta}{\tau_\mathrm{R}}\right), \tag{1}$$

where A_R and A_I are the mass numbers of R and I, $X_\mathrm{I}^\odot$ is the solar mass fraction of I [30], Δ is the time between the CCSN explosion and incorporation of R into early SS solids, and τ_R is the lifetime of R.

Table 1 gives the mass yields of ^{10}Be, ^{26}Al, ^{36}Cl, ^{41}Ca, ^{53}Mn, ^{60}Fe, ^{107}Pd, ^{135}Cs, ^{182}Hf, and ^{205}Pb for the 11.8 $M_\odot$ model. A comparison of equation (1) to the observed value, including uncertainties [22, 31–45], yields a band of allowed f and Δ for each SLR. Simultaneous explanation of SLRs then requires the corresponding bands to overlap. Figure 2 shows a region of concordance for ^{10}Be, ^{41}Ca, and ^{107}Pd. This fixes f and Δ, allowing us to estimate the contributions from the 11.8 $M_\odot$ CCSN to other SLRs. The Case 1 contributions to ^{26}Al, ^{36}Cl, ^{53}Mn, ^{60}Fe, ^{135}Cs, ^{182}Hf, and ^{205}Pb in Table 1 correspond to $f \sim 5 \times 10^{-4}$ and $\Delta \sim 1$ Myr, the approximate best-fit point indicated by the filled circle in Fig. 2.

The slow-neutron-capture (s) process product ^{182}Hf is of special interest, as the yield

of this SLR is sensitive to the β-decay rate of ^{181}Hf, which may be affected by thermally-populated low-lying excited states under stellar conditions. We treat the excited-state contribution as an uncertainty [46], allowing the rate to vary between the laboratory value and the theoretical estimate of Ref. [47] with excited states. (The latter is numerically close to updated estimates with uncertainties [46].) The yield obtained with the laboratory rate accounts for almost all of the ^{182}Hf in the early SS. This removes a conflict with data on the SLR ^{129}I that arises when ^{182}Hf is attributed to the rapid neutron-capture (r) process [46, 48].

Role of Fallback

The Case 1 results of Table 1 are consistent with the meteoritic data on ^{26}Al, ^{36}Cl, ^{135}Cs, ^{182}Hf, and ^{205}Pb, as the contributions do not exceed the measured values. In contrast, although the production of ^{53}Mn and ^{60}Fe is greatly reduced in low-mass CCSNe, the ^{53}Mn contribution remains a factor of 60 too large while ^{60}Fe is compatible only with the larger of the two observed values (see Table 1). Both of these SLRs originate from zones deep within the 11.8 $M_\odot$ star: ^{53}Mn is produced in the innermost $10^{-2}\,M_\odot$ of the shocked material, while $\sim 90\%$ of the ^{60}Fe is associated with the innermost $0.12\,M_\odot$. Because of the low explosion energy used here based on simulations [26], the expected fallback of the innermost shocked zones onto the protoneutron star [49] provides a natural explanation for the discrepancies: most of the produced ^{53}Mn and, possibly, ^{60}Fe is not ejected. In Case 2 of Table 1, where only 1.5% of the innermost $1.02 \times 10^{-2}\,M_\odot$ is ejected, ^{53}Mn/^{55}Mn is reduced to its measured value $(6.28 \pm 0.66) \times 10^{-6}$ [38], while other SLR contributions are largely unaffected. In Case 3, where only 1.5% of the innermost $0.116\,M_\odot$ is ejected, additional large reductions (a factor of ~ 10) are found for ^{60}Fe and ^{182}Hf, accompanied by smaller decreases (a factor of ~ 2) in ^{26}Al, ^{36}Cl, ^{135}Cs, and ^{205}Pb.

Case 3 represents the limit of reducing ^{53}Mn and ^{60}Fe without affecting the concordance among ^{10}Be, ^{41}Ca, and ^{107}Pd (see Supplementary Fig. 1, Supplementary Discussion). Were the lower observed value for ^{60}Fe [39] proven correct, we would have to either reduce its yield by examining the significant nuclear and stellar physics uncertainties [50, 51] or use even more substantial fallback and reconsider the low-mass CCSN contributions to SLRs. Because of the correlated effects of fallback on ^{60}Fe and ^{182}Hf, more fallback would also rule out an attractive explanation for the latter, as described above. Note that the fallback assumed for Cases 2 and 3 is far below that invoked for high-mass CCSNe in Ref. [8] to

account for ^{26}Al, ^{41}Ca, ^{53}Mn, and the higher observed value of ^{60}Fe.

If, however, the higher ^{60}Fe value [40] is correct, then a plausible scenario like Case 2, where SS formation was triggered by a low-mass CCSN with modest fallback, would be in reasonable agreement with the data on ^{10}Be, ^{41}Ca, ^{53}Mn, ^{60}Fe, and ^{107}Pd. The nuclear forensics, notably the rapidly decaying ^{41}Ca, determines the delay between the CCSN explosion and incorporation of SLRs into early SS solids, $\Delta \sim 1$ Myr. The deduced fraction of CCSN material injected into the protosolar cloud, $f \sim 5 \times 10^{-4}$, is consistent with estimates based on simulations of ejecta interacting with dense gas clouds [4–6] (see Supplementary Discussion). There is also an implicit connection to the CCSN explosion energy, which influences fallback in hydrodynamic models.

Discussion

In addition to neutrino-induced production, a low-mass CCSN can make ^{10}Be through CRs associated with its remnant evolution [20]. However, the yield of this second source is modest (see Supplementary Discussion). The net yield in the ISM trapped within the remnant is limited by the amount of this ISM. Production within the general protosolar cloud during its initial contact with the remnant (i.e., prior to thorough mixing of the injected material) would also be expected, and the yield could possibly account for ^{10}Be/^{9}Be $\sim 3 \times 10^{-4}$ in FUN-CAIs [20]. However, FUN-CAIs are rare, and their ^{10}Be inventory may be more consistent with local production by the CCSN CRs. Taking the net CR contribution averaged over the protosolar cloud to be ^{10}Be/^{9}Be $\sim 10^{-4}$, a value that we argue is more consistent with long-term production by Galactic CRs [20], we add the neutrino-produced ^{10}Be/^{9}Be $\sim (5.2\text{–}6.4) \times 10^{-4}$ (see Table 1) from the CCSN to obtain ^{10}Be/^{9}Be $\sim (6.2\text{–}7.4) \times 10^{-4}$, which is in accord with ^{10}Be/^{9}Be $= (7.5 \pm 2.5) \times 10^{-4}$ observed in canonical CAIs. In general, we consider that neutrino-induced production provided the baseline ^{10}Be inventory in these samples and the observed variations [14, 16, 18, 19] can be largely attributed to local production by SEPs.

Our proposal that a low-mass CCSN trigger provided the bulk of the ^{10}Be inventory in the early SS has several important features: (1) the relevant neutrino and CCSN physics is known reasonably well, and the uncertainty in the ^{10}Be yield is estimated here to be within a factor of ~ 2; (2) the production of both ^{10}Be and ^{41}Ca is in agreement with observations

[36, 37], a result difficult to achieve by SEPs [19]; and (3) the yield pattern of Li, Be, and B isotopes (see Supplementary Table 4) is distinctive, with predominant production of ^{7}Li and ^{11}B and differing greatly from patterns of production by CRs and SEPs, so that precise meteoritic data might provide distinguishing tests (see Supplementary Discussion).

We emphasize that while ^{53}Mn and ^{60}Fe production is greatly reduced in a low-mass CCSN, some fallback is still required to explain the meteoritic data. The fallback solution works well for ^{53}Mn (see Table 1). When somewhat different meteoritic values of ^{53}Mn/^{55}Mn [52, 53] are used, only the ejected fractions of the innermost shocked material need to be adjusted accordingly. The case of ^{60}Fe is more complicated. The meteoritic measurements are difficult, especially in view of a recent study showing the mobility of Fe and Ni in the relevant samples [54]. Another recent study gave $5 \times 10^{-8} \lesssim {}^{60}\mathrm{Fe}/{}^{56}\mathrm{Fe} \lesssim 2.6 \times 10^{-7}$ [55], which may be accounted for by Case 3 of our model (see Table 1). However, were ^{60}Fe/^{56}Fe $\sim 10^{-8}$ [39], currently preferred by many workers, to be confirmed, we would have to conclude that either the present ^{60}Fe yield of the low-mass CCSN is wrong or its contributions to SLRs must be reconsidered.

Several other issues with our proposed low-mass CCSN trigger merit discussion. Table 1 shows that such a CCSN underproduces ^{26}Al, ^{36}Cl, and ^{135}Cs to varying degrees. We consider that the ISM swept up by the CCSN shock wave prior to triggering the collapse of the protosolar cloud might have been enriched with ^{26}Al by nearby massive stars. To avoid complications with ^{53}Mn and ^{60}Fe, we propose that these stars might have exploded only weakly or not at all [49], but contributed ^{26}Al through their winds. The total amount of swept-up ^{26}Al needed to be $\sim 10^{-5}\,M_{\odot}$ (see Table 2), which could have been provided by winds from stars of $\gtrsim 35\,M_{\odot}$ [50], possibly in connection with an evolving giant molecular cloud [56]. Winds from massive stars may also have contributed to ^{41}Ca and ^{135}Cs [57]. However, the wind contribution to ^{41}Ca might be neglected given the rapid decay of this SLR over the interval of ~ 1 Myr between the onset of collapse of the protosolar cloud and incorporation of SLRs into early SS solids (see Supplementary Discussion). We agree with previous studies that ^{36}Cl was probably produced by SEPs after most of the initial ^{26}Al had decayed [34, 35]. The corresponding late irradiation would not have caused problematic coproduction of other SLRs, especially ^{10}Be, ^{26}Al, and ^{53}Mn, if it occurred in a reservoir enriched with volatile elements such as chlorine, a major target for producing ^{36}Cl [35].

Our calculations do not include nucleosynthesis in the neutrino-heated ejecta from the

protoneutron star, where some form of the r process may take place [58, 59]. This is a potential source of the SLR ^{129}I. As emphasized above, a low-mass CCSN would alter the SS ratios of stable isotopes of e.g., Mg, Si, Ca, and Fe only at levels of $\lesssim 1\%$ (see Supplementary Discussion), consistent with meteoritic constraints [3]. Nonetheless, Cases 2 and 3 with fallback would produce anomalies in ^{54}Cr, ^{58}Fe, and ^{64}Ni at levels of $\sim 10^{-3}$ as observed in meteorites (see Supplementary Discussion). As there are few satisfactory explanations of these anomalies [60], this provides circumstantial support for the fallback scenario required by the ^{53}Mn and ^{60}Fe data.

We conclude that a low-mass CCSN is a promising trigger for SS formation. Such a trigger is plausible because the lifetime of ~ 20 Myr for the CCSN progenitor is compatible with the duration of star formation in giant molecular clouds [61]. Further progress depends on resolving discrepancies in ^{60}Fe abundance determinations, clarifying the nuclear physics of ^{181}Hf decay, and studying the evolution of additional low-mass CCSN progenitors and their explosion, especially quantifying fallback through multi-dimensional models. In addition, the overall scenario proposed here to explain the SLRs in the early SS requires comprehensive modeling of ^{26}Al enrichment by winds from massive stars in an evolving giant molecular cloud, evolution of a low-mass CCSN remnant and the resulting CR production and interaction, and irradiation by SEPs associated with activities of the proto-Sun. Finally, tests of the low-mass CCSN trigger by precise measurements of Li, Be, and B isotopes in meteorites are highly desirable (see Supplementary Discussion).

Data Availability

The data that support the findings of this study are available from the corresponding author upon reasonable request.

[1] Cameron, A. G. W. & Truran, J. W. The supernova trigger for formation of the solar system. *Icarus* **30**, 447–461 (1977).

[2] Lee, T., Papanastassiou, D. A. & Wasserburg, G. J. Correction [to "Demonstration of ^{26}Mg excess in Allende and evidence for ^{26}Al"]. *Geophys. Res. Lett.* **3**, 109–112 (1976).

[3] Wasserburg, G. J., Busso, M., Gallino, R. & Nollett, K. M. Short-lived nuclei in the early solar system: Possible AGB sources. *Nucl. Phys. A* **777**, 5–69 (2006).

[4] Boss, A. P. & Keiser, S. A. Who pulled the trigger: A supernova or an asymptotic giant branch star? *Astrophy. J.* **717**, L1–L5 (2010).

[5] Boss, A. P. & Keiser, S. A. Triggering collapse of the presolar dense cloud core and injecting short-lived radioisotopes with a shock wave. III. Rotating three-dimensional cloud cores. *Astrophys. J.* **788**, 20 (2014).

[6] Boss, A. P. & Keiser, S. A. Triggering collapse of the presolar dense cloud core and injecting short-lived radioisotopes with a shock wave. IV. Effects of rotational axis orientation. *Astrophys. J.* **809**, 103 (2015).

[7] Meyer, B. S. & Clayton, D. D. Short-lived radioactivities and the birth of the sun. *Space Science Reviews* **92**, 133–152 (2000).

[8] Takigawa, A. *et al.* Injection of short-lived radionuclides into the early solar system from a faint supernova with mixing fallback. *Astrophys. J.* **688**, 1382–1387 (2008).

[9] Desch, S. J., Connolly, H. C., Jr. & Srinivasan, G. An interstellar origin for the beryllium 10 in calcium-rich, aluminum-rich inclusions. *Astrophys. J.* **602**, 528–542 (2004).

[10] Gounelle, M. *et al.* Extinct radioactivities and protosolar cosmic rays: Self-shielding and light elements. *Astrophys. J.* **548**, 1051–1070 (2001).

[11] Gounelle, M. *et al.* The irradiation origin of beryllium radioisotopes and other short-lived radionuclides. *Astrophys. J.* **640**, 1163–1170 (2006).

[12] Yoshida, T. *et al.* Neutrino-nucleus reaction cross sections for light element synthesis in supernova explosions. *Astrophys. J.* **686**, 448–466 (2008).

[13] Cyburt, R. H. *et al.* The JINA REACLIB database: Its recent updates and impact on type-I X-ray bursts. *Astrophys. J. Suppl. Ser.* **189**, 240–252 (2010).

[14] McKeegan, K. D., Chaussidon, M. & Robert, F. Incorporation of short-lived ^{10}Be in a calcium-aluminum-rich inclusion from the Allende meteorite. *Science* **289**, 1334–1337 (2000).

[15] Marhas, K. K., Goswami, J. N. & Davis, A. M. Short-lived nuclides in hibonite grains from Murchison: Evidence for solar system evolution. *Science* **298**, 2182–2185 (2002).

[16] MacPherson, G. J., Huss, G. R. & Davis, A. M. Extinct ^{10}Be in Type A calcium-aluminum-rich inclusions from CV chondrites. *Geochim. Cosmochim. Acta* **67**, 3165–3179 (2003).

[17] Liu, M.-C., Nittler, L. R., Alexander, C. M. O. & Lee, T. Lithium-beryllium-boron isotopic

compositions in meteoritic hibonite: Implications for origin of ^{10}Be and early solar system irradiation. *Astrophys. J.* **719**, L99–L103 (2010).

[18] Wielandt, D. *et al.* Evidence for multiple sources of ^{10}Be in the early solar system. *Astrophys. J.* **748**, L25 (2012).

[19] Srinivasan, G. & Chaussidon, M. Constraints on ^{10}Be and ^{41}Ca distribution in the early solar system from ^{26}Al and ^{10}Be studies of Efremovka CAIs. *Earth Planet. Sci. Lett.* **374**, 11–23 (2013).

[20] Tatischeff, V., Duprat, J. & de Séréville, N. Light-element nucleosynthesis in a molecular cloud interacting with a supernova remnant and the origin of beryllium-10 in the protosolar nebula. *Astrophys. J.* **796**, 124 (2014).

[21] Duprat, J. & Tatischeff, V. Energetic constraints on in situ production of short-lived radionuclei in the early solar system. *Astrophys. J.* **671**, L69–L72 (2007).

[22] Dauphas, N. & Chaussidon, M. A perspective from extinct radionuclides on a young stellar object: The sun and its accretion disk. *Annu. Rev. Earth Planet. Sci.* **39**, 351–386 (2011).

[23] Weaver, T. A., Zimmerman, G. B. & Woosley, S. E. Presupernova evolution of massive stars. *Astrophys. J.* **225**, 1021–1029 (1978).

[24] Rauscher, T., Heger, A., Hoffman, R. D. & Woosley, S. E. Hydrostatic and explosive nucleosynthesis in massive stars using improved nuclear and stellar physics. *Nucl. Phys. A* **718**, 463 – 465 (2003).

[25] Bruenn, S. W. *et al.* Axisymmetric ab initio core-collapse supernova simulations of 12–25 $M_\odot$ stars. *Astrophys. J.* **767**, L6 (2013).

[26] Melson, T., Janka, H.-T. & Marek, A. Neutrino-driven supernova of a low-mass iron-core progenitor boosted by three-dimensional turbulent convection. *Astrophys. J.* **801**, L24 (2015).

[27] Müller, B. & Janka, H.-T. A new multi-dimensional general relativistic neutrino hydrodynamics code for core-collapse supernovae. IV. The neutrino signal. *Astrophys. J.* **788**, 82 (2014).

[28] Yüksel, H. & Beacom, J. F. Neutrino spectrum from SN 1987A and from cosmic supernovae. *Phys. Rev. D* **76**, 083007 (2007).

[29] Heger, A. *et al.* Neutrino nucleosynthesis. *Phys. Lett. B* **606**, 258–264 (2005).

[30] Asplund, M., Grevesse, N., Sauval, A. J. & Scott, P. The chemical composition of the sun. *Annu. Rev. Astron. Astrophys.* **47**, 481–522 (2009).

[31] Davis, A. M. & McKeegan, K. D. Short-lived radionuclides and early solar system chronology. In *Meteorites and Cosmochemical Processes, Treatise of Geochemistry*, vol. 1, 361–395 (Elsevier, 2014).

[32] Jacobsen, B. *et al.* ^{26}Al-^{26}Mg and ^{207}Pb-^{206}Pb systematics of Allende CAIs: Canonical solar initial ^{26}Al/^{27}Al ratio reinstated. *Earth Planet. Sci. Lett.* **272**, 353–364 (2008).

[33] Lin, Y., Guan, Y., Leshin, L. A., Ouyang, Z. & Wang, D. Short-lived chlorine-36 in a Ca- and Al-rich inclusion from the Ningqiang carbonaceous chondrite. *Proc. Natl. Acad. Sci. U.S.A.* **102**, 1306–1311 (2005).

[34] Hsu, W., Guan, Y., Leshin, L. A., Ushikubo, T. & Wasserburg, G. J. A late episode of irradiation in the early solar system: Evidence from extinct ^{36}Cl and ^{26}Al in meteorites. *Astrophys. J.* **640**, 525–529 (2006).

[35] Jacobsen, B. *et al.* Formation of the short-lived radionuclide ^{36}Cl in the protoplanetary disk during late-stage irradiation of a volatile-rich reservoir. *Astrophy. J.* **731**, L28 (2011).

[36] Ito, M., Nagasawa, H. & Yurimoto, H. A study of Mg and K isotopes in Allende CAIs: Implications to the time scale for the multiple heating processes. *Meteorit. Planet. Sci.* **41**, 1871–1881 (2006).

[37] Liu, M.-C., Chaussidon, M., Srinivasan, G. & McKeegan, K. D. A lower initial abundance of short-lived ^{41}Ca in the early solar system and its implications for solar system formation. *Astrophys. J.* **761**, 137 (2012).

[38] Trinquier, A., Birck, J.-L., Allègre, C. J., Göpel, C. & Ulfbeck, D. ^{53}Mn-^{53}Cr systematics of the early solar system revisited. *Geochim. Cosmochim. Acta* **72**, 5146–5163 (2008).

[39] Tang, H. & Dauphas, N. Low ^{60}Fe abundance in Semarkona and Sahara 99555. *Astrophys. J.* **802**, 22 (2015).

[40] Mishra, R. K. & Goswami, J. N. Fe-Ni and Al-Mg isotope records in UOC chondrules: Plausible stellar source of ^{60}Fe and other short-lived nuclides in the early Solar System. *Geochim. Cosmochim. Acta* **132**, 440–457 (2014).

[41] Schönbächler, M., Carlson, R. W., Horan, M. F., Mock, T. D. & Hauri, E. H. Silver isotope variations in chondrites: Volatile depletion and the initial ^{107}Pd abundance of the solar system. *Geochim. Cosmochim. Acta* **72**, 5330–5341 (2008).

[42] Hidaka, H., Ohta, Y., Yoneda, S. & DeLaeter, J. R. Isotopic search for live ^{135}Cs in the early solar system and possibility of ^{135}Cs-^{135}Ba chronometer. *Earth Planet. Sci. Lett.* **193**, 459–466

(2001).

[43] Burkhardt, C. *et al.* Hf-W mineral isochron for Ca,Al-rich inclusions: Age of the solar system and the timing of core formation in planetesimals. *Geochim. Cosmochim. Acta* **72**, 6177–6197 (2008).

[44] Nielsen, S. G., Rehkämper, M. & Halliday, A. N. Large thallium isotopic variations in iron meteorites and evidence for lead-205 in the early solar system. *Geochim. Cosmochim. Acta* **70**, 2643–2657 (2006).

[45] Baker, R. G. A., Schönbächler, M., Rehkämper, M., Williams, H. M. & Halliday, A. N. The thallium isotope composition of carbonaceous chondrites — New evidence for live ^{205}Pb in the early solar system. *Earth Planet. Sci. Lett.* **291**, 39–47 (2010).

[46] Lugaro, M. *et al.* Stellar origin of the ^{182}Hf cosmochronometer and the presolar history of solar system matter. *Science* **345**, 650–653 (2014).

[47] Takahashi, K. & Yokoi, K. Beta-decay rates of highly ionized heavy atoms in stellar interiors. *At. Data Nucl. Data Tables* **36**, 375–409 (1987).

[48] Wasserburg, G. J., Busso, M. & Gallino, R. Abundances of actinides and short-lived nonactinides in the interstellar medium: Diverse supernova sources for the r-processes. *Astrophys. J.* **466**, L109–L113 (1996).

[49] Zhang, W., Woosley, S. E. & Heger, A. Fallback and black hole production in massive stars. *Astrophys. J.* **679**, 639–654 (2008).

[50] Limongi, M. & Chieffi, A. The nucleosynthesis of ^{26}Al and ^{60}Fe in solar metallicity stars extending in mass from 11 to 120 $M_{\odot}$: The hydrostatic and explosive contributions. *Astrophys. J.* **647**, 483–500 (2006).

[51] Woosley, S. E. & Heger, A. Nucleosynthesis and remnants in massive stars of solar metallicity. *Phys. Rep.* **442**, 269–283 (2007).

[52] Nyquist, L. E., Kleine, T., Shih, C.-Y. & Reese, Y. D. The distribution of short-lived radioisotopes in the early solar system and the chronology of asteroid accretion, differentiation, and secondary mineralization. *Geochim. Cosmochim. Acta* **73**, 5115–5136 (2009).

[53] Yamashita, K., Maruyama, S., Yamakawa, A. & Nakamura, E. ^{53}Mn-^{53}Cr chronometry of CB chondrite: Evidence for uniform distribution of ^{53}Mn in the early solar system. *Astrophy. J.* **723**, 20–24 (2010).

[54] Telus, M. *et al.* Mobility of iron and nickel at low temperatures: Implications for ^{60}Fe-^{60}Ni

systematics of chondrules from unequilibrated ordinary chondrites. *Geochim. Cosmochim. Acta* **178**, 87–105 (2016).

[55] Telus, M., Huss, G. R., Nagashima, K., Ogliore, R. C. & Tachibana, S. ^{60}Fe-^{60}Ni systematics of chondrules: Constraints from in situ analyses. In *Lunar and Planetary Science Conference*, vol. 47, 1816 (Lunar and Planetary Institute, 2016).

[56] Vasileiadis, A., Nordlund, Å. & Bizzarro, M. Abundance of ^{26}Al and ^{60}Fe in evolving giant molecular clouds. *Astrophys. J.* **769**, L8 (2013).

[57] Arnould, M., Goriely, S. & Meynet, G. The production of short-lived radionuclides by new non-rotating and rotating Wolf-Rayet model stars. *Astron. Astrophys.* **453**, 653–659 (2006).

[58] Woosley, S. E., Wilson, J. R., Mathews, G. J., Hoffman, R. D. & Meyer, B. S. The r-process and neutrino-heated supernova ejecta. *Astrophys. J.* **433**, 229–246 (1994).

[59] Wanajo, S., Janka, H.-T. & Müller, B. Electron-capture supernovae as the origin of elements beyond iron. *Astrophys. J.* **726**, L15 (2011).

[60] Wasserburg, G. J., Trippella, O. & Busso, M. Isotope anomalies in the Fe-group elements in meteorites and connections to nucleosynthesis in AGB stars. *Astrophys. J.* **805**, 7 (2015).

[61] Murray, N. Star formation efficiencies and lifetimes of giant molecular clouds in the Milky Way. *Astrophys. J.* **729**, 133 (2011).

Acknowledgements

We acknowledge helpful discussions with Bernhard Müller and the late Jerry Wasserburg. We thank Takashi Yoshida for communications regarding Ref. [12]. This work was supported in part by the US DOE [DE-FG02-87ER40328 (UM), de-sc00046548 (Berkeley), and DE-AC02-98CH10886 (LBL)], the US NSF [PHY-1430152 (JINA-CEE)], and ARC Future Fellowship FT120100363 (AH).

Author contributions

P.B. and Y.-Z.Q. designed the work. P.B. ran the models with help from A.H. All the authors discussed the results and contributed to the writing of the manuscript.

Competing financial interests

The authors declare no competing financial interests.

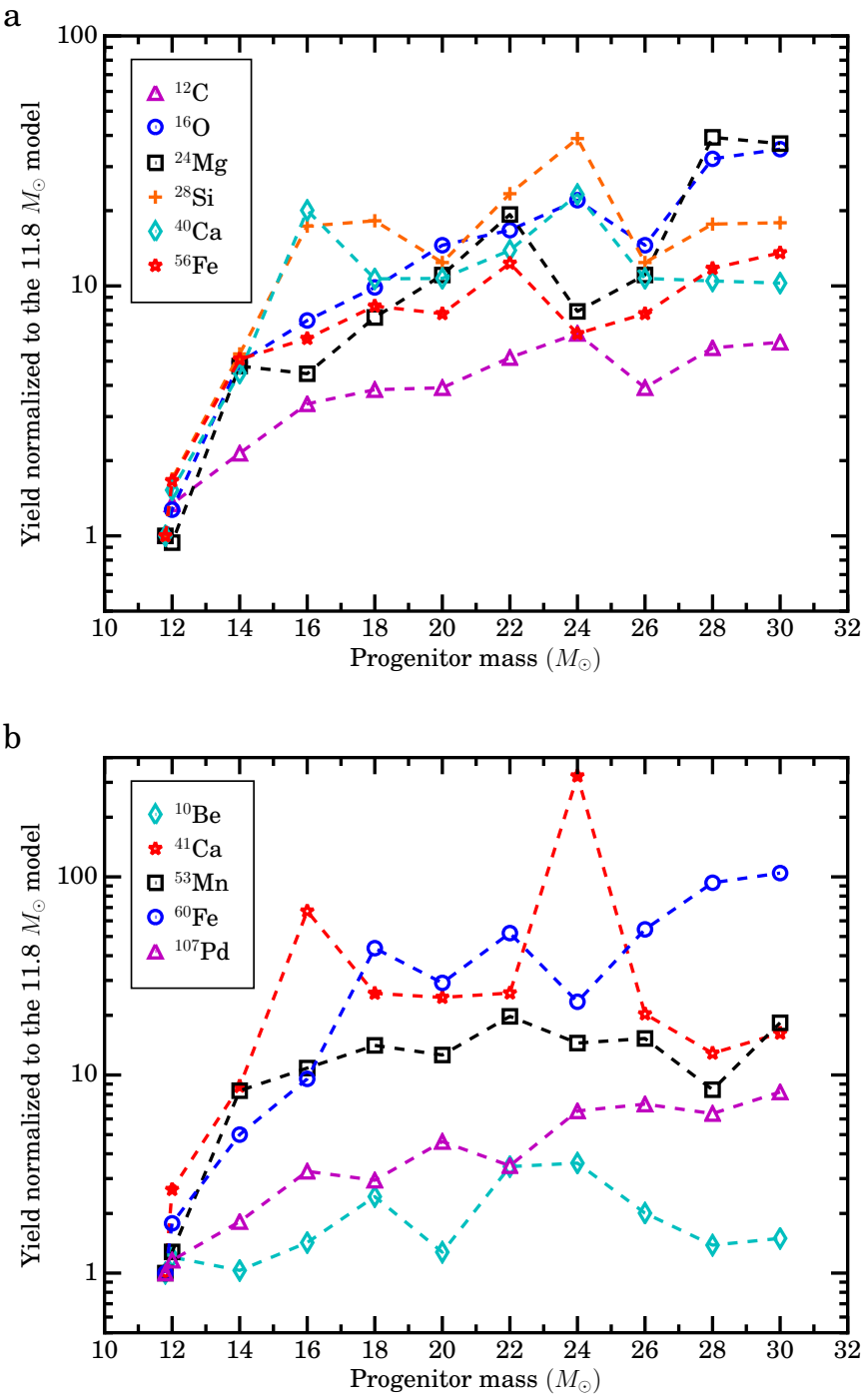

FIG. 1: Nucleosynthetic yields as functions of the supernova progenitor's mass. Selected yields of (a) stable isotopes and (b) short-lived radionuclides are shown, normalized to the 11.8-solar-mass model, for Case 1 with no fallback.

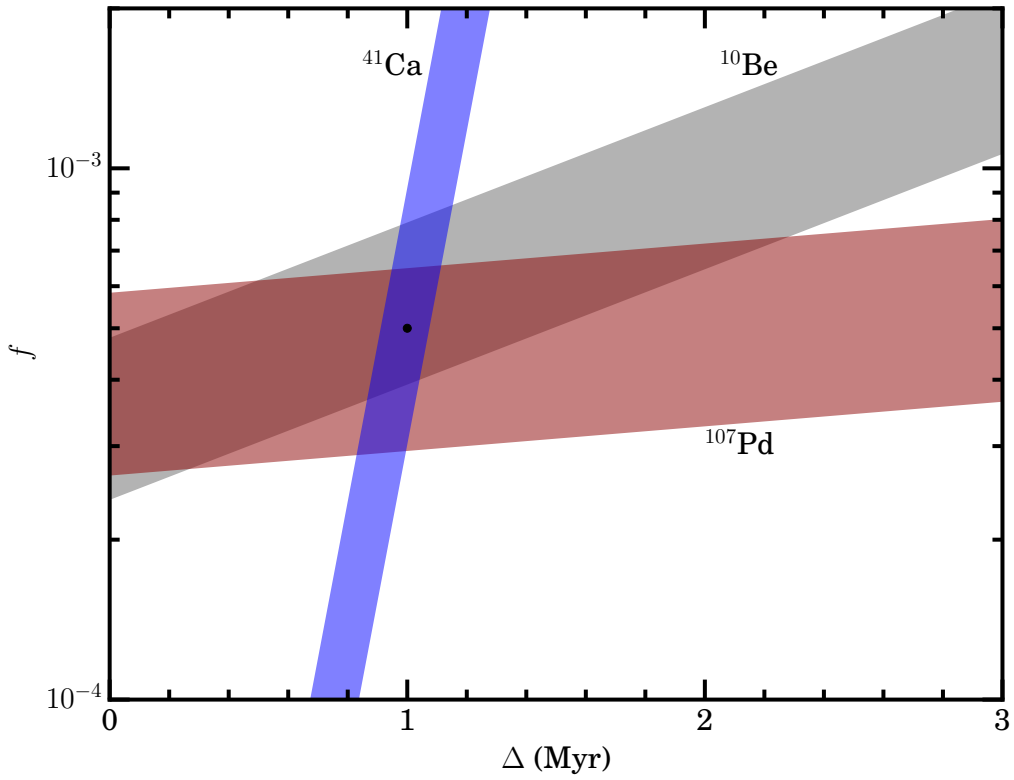

FIG. 2: Relations between parameters characterizing the core-collapse supernova trigger. The parameter f denotes the fraction of the yields of short-lived nuclides incorporated into the proto-solar cloud, per solar mass. The parameter Δ denotes the time between the supernova explosion and incorporation of short-lived nuclides into early solar system solids. Results are calculated from equation (1) using yields for the 11.8-solar-mass model with no fallback (Case 1) and meteoritic data for ^{10}Be, ^{41}Ca, and ^{107}Pd with 2σ uncertainties (see Table 1). The filled circle at $f \sim 5 \times 10^{-4}$ and $\Delta \sim 1$ Myr is the approximate best-fit point within the overlap region.

Table 1: Yields of short-lived radionuclides from an 11.8-solar-mass core-collapse supernova

R/I	$\tau_{\rm R}$	$Y_{\rm R}$	$X_{\rm I}^{\odot}$	$(N_{\rm R}/N_{\rm I})_{\rm ESS}$			
	(Myr)	($M_{\odot}$)		Data	Case 1	Case 2	Case 3
^{10}Be/^{9}Be	2.00	3.26(−10)	1.40(−10)	$(7.5 \pm 2.5)(-4)$	6.35(−4)	6.35(−4)	5.20(−4)
^{26}Al/^{27}Al	1.03	2.91(−6)	5.65(−5)	$(5.23 \pm 0.13)(-5)$	1.02(−5)	9.90(−6)	5.77(−6)
^{36}Cl/^{35}Cl	0.434	1.44(−7)	3.50(−6)	$\sim$ (3–20)(−6)	2.00(−6)	1.45(−6)	6.15(−7)
^{41}Ca/^{40}Ca	0.147	3.66(−7)	5.88(−5)	$(4.1 \pm 2.0)(-9)$	3.40(−9)	2.74(−9)	2.26(−9)
^{53}Mn/^{55}Mn	5.40	1.22(−5)	1.29(−5)	$(6.28 \pm 0.66)(-6)$	4.04(−4)	6.39(−6)	6.16(−6)
^{60}Fe/^{56}Fe	3.78	3.08(−6)	1.12(−3)	$\sim 1(-8); (5–10)(-7)$	9.80(−7)	9.80(−7)	1.10(−7)
^{107}Pd/^{108}Pd	9.38	1.37(−10)	9.92(−10)	$(5.9 \pm 2.2)(-5)$	6.27(−5)	6.27(−5)	5.72(−5)
^{135}Cs/^{133}Cs	3.32	2.56(−10)	1.24(−9)	$\sim 5(-4)$	7.51(−5)	7.51(−5)	3.18(−5)
^{182}Hf/^{180}Hf	12.84	4.04(−11)	2.52(−10)	$(9.72 \pm 0.44)(-5)$	7.36(−5)	7.36(−5)	6.34(−6)
		8.84(−12)			1.60(−5)	1.60(−5)	2.37(−6)
^{205}Pb/^{204}Pb	24.96	9.20(−11)	3.47(−10)	$\sim 1(-4); 1(-3)$	1.27(−4)	1.27(−4)	7.78(−5)

Comparisons are made to the corresponding isotopic ratios deduced from meteoritic data. Case 1 estimates are calculated from equation (1) using the approximate best-fit f and Δ of Fig. 2, assuming no fallback. The higher and lower yields for ^{182}Hf are obtained from the laboratory and estimated stellar decay rates [47] of ^{181}Hf, respectively. Case 2 (3) is a fallback scenario in which only 1.5% of the innermost 1.02×10^{-2} solar mass (0.116 solar mass) of shocked material is ejected. With guidance from Refs. [22, 31], well-determined data are quoted with 2σ errors, while data with large uncertainties are preceded by "$\sim$". Note that $x(-y)$ denotes $x \times 10^{-y}$. Data references are: ^{10}Be [14, 16, 18, 19], ^{26}Al [2, 32], ^{36}Cl [33–35], ^{41}Ca [36, 37], ^{53}Mn [38], ^{60}Fe [39, 40], ^{107}Pd [41], ^{135}Cs [42], ^{182}Hf [43], ^{205}Pb [44, 45].

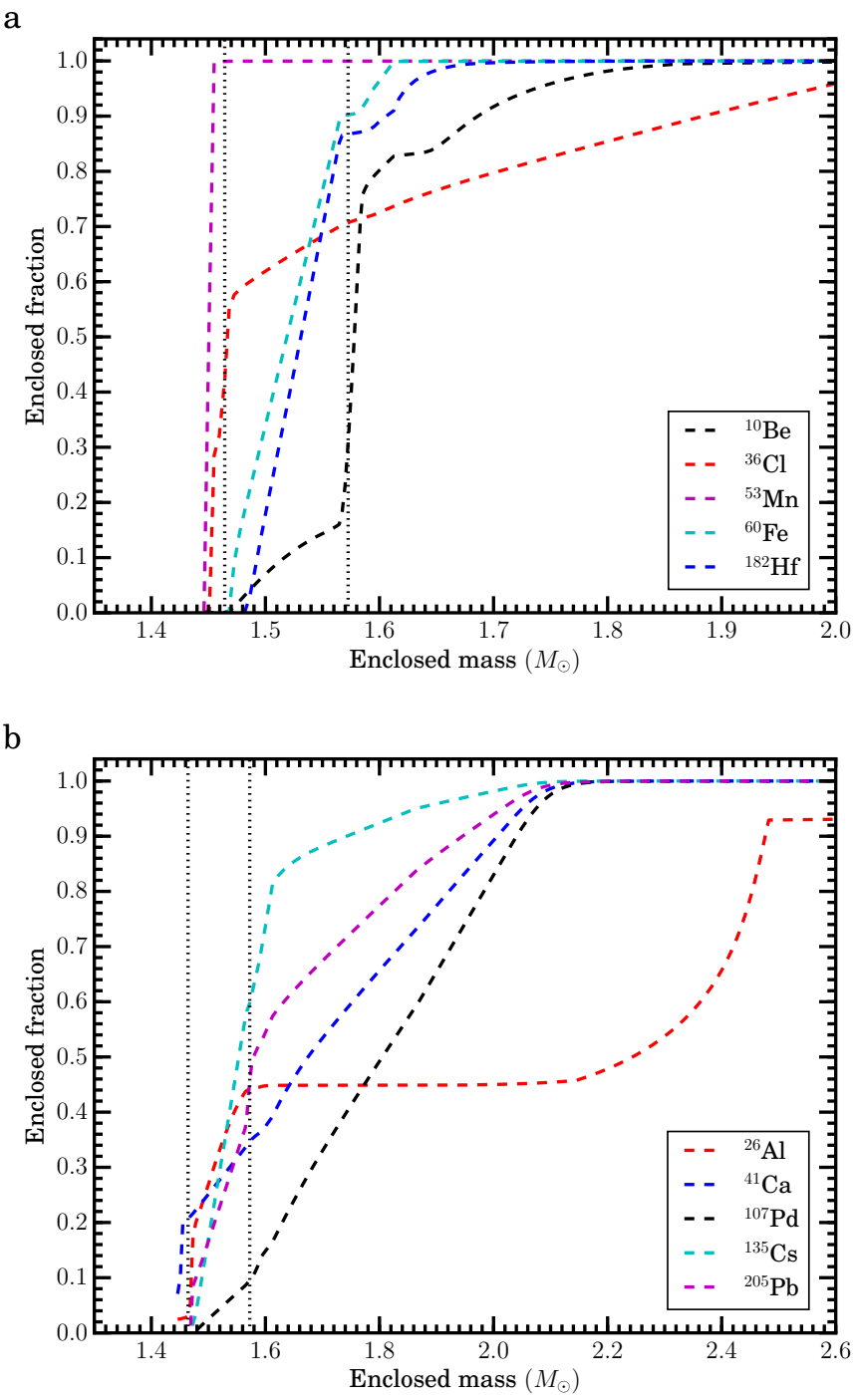

Supplementary Figure 1: Enclosed fraction of the total yield of each short-lived radionuclide as a function of the enclosed stellar mass for the 11.8-solar-mass model with no fallback (Case 1). The left and right vertical lines indicate the boundary between fallback and ejected material for Cases 2 and 3, respectively.

Supplementary Table 1: Supernova contributions to short-lived radionuclides in the early solar system from the 20- and 30-solar-mass models

R/I	$20\,M_\odot$	$30\,M_\odot$
^{10}Be/^{9}Be	7.39(−5)	3.70(−5)
^{26}Al/^{27}Al	5.64(−5)	5.17(−5)
^{36}Cl/^{35}Cl	2.89(−6)	1.37(−6)
^{41}Ca/^{40}Ca	4.95(−9)	4.21(−9)
^{53}Mn/^{55}Mn	6.24(−6)	6.40(−6)
^{60}Fe/^{56}Fe	1.04(−6)	9.48(−7)
^{107}Pd/^{108}Pd	3.02(−4)	1.47(−4)
^{135}Cs/^{133}Cs	3.01(−4)	5.85(−5)
^{182}Hf/^{180}Hf	4.54(−5)	7.52(−6)
^{205}Pb/^{204}Pb	4.76(−04)	1.35(−4)

Fallback scenarios similar to those of Ref. [S1] are assumed. Values for ^{182}Hf are obtained from the estimated stellar decay rate of ^{181}Hf [S2]. Note that ^{107}Pd is overproduced and $x(-y)$ denotes $x \times 10^{-y}$.

Supplementary Table 2: Yields of major stable isotopes for the 11.8-solar-mass model with no fallback (Case 1)

Isotope	Yield ($M_\odot$)	Isotope	Yield ($M_\odot$)	Isotope	Yield ($M_\odot$)
^{12}C	5.75(−2)	^{33}S	3.39(−5)	^{54}Cr	5.08(−6)
^{13}C	6.98(−4)	^{34}S	1.91(−4)	^{54}Fe	8.58(−4)
^{14}N	2.68(−2)	^{36}S	1.18(−6)	^{56}Fe	1.77(−2)
^{15}N	1.96(−5)	^{40}Ca	7.28(−4)	^{57}Fe	5.51(−4)
^{16}O	1.43(−1)	^{42}Ca	4.00(−6)	^{58}Fe	9.23(−5)
^{17}O	5.41(−5)	^{43}Ca	1.05(−6)	^{58}Ni	6.95(−4)
^{18}O	7.46(−4)	^{44}Ca	1.64(−5)	^{60}Ni	3.53(−4)
^{20}Ne	3.55(−2)	^{46}Ca	5.36(−8)	^{61}Ni	2.76(−5)
^{21}Ne	1.17(−4)	^{48}Ca	1.21(−6)	^{62}Ni	8.73(−5)
^{22}Ne	3.16(−3)	^{46}Ti	2.22(−6)	^{64}Ni	2.00(−5)
^{24}Mg	8.60(−3)	^{47}Ti	2.29(−6)	^{64}Zn	1.03(−5)
^{25}Mg	1.50(−3)	^{48}Ti	3.03(−5)	^{66}Zn	8.75(−6)
^{26}Mg	1.61(−3)	^{49}Ti	2.19(−6)	^{67}Zn	1.40(−6)
^{28}Si	9.11(−3)	^{50}Ti	1.80(−6)	^{68}Zn	5.64(−6)
^{29}Si	4.38(−4)	^{50}Cr	9.32(−6)	^{70}Zn	1.63(−7)
^{30}Si	4.29(−4)	^{52}Cr	2.15(−4)		
^{32}S	4.71(−3)	^{53}Cr	2.74(−5)		

Note that $x(-y)$ denotes $x \times 10^{-y}$.

Supplementary Table 3: Percentage of the solar system inventory of major stable isotopes contributed by the 11.8-solar-mass model

Isotope	Case 1	Case 2	Case 3	Isotope	Case 1	Case 2	Case 3
^{12}C	1.16	1.16	1.10	^{48}Ca	0.45	0.45	0.44
^{13}C	1.16	1.16	1.16	^{46}Ti	0.46	0.46	0.45
^{14}N	1.82	1.82	1.82	^{47}Ti	0.52	0.45	0.44
^{15}N	0.33	0.33	0.22	^{48}Ti	0.68	0.44	0.44
^{16}O	1.18	1.18	0.56	^{49}Ti	0.65	0.51	0.48
^{17}O	1.10	1.10	1.06	^{50}Ti	0.55	0.55	0.48
^{18}O	2.72	2.72	2.72	^{50}Cr	0.63	0.44	0.44
^{20}Ne	1.44	1.44	0.48	^{52}Cr	0.73	0.45	0.44
^{21}Ne	1.89	1.89	0.98	^{53}Cr	0.80	0.45	0.45
^{22}Ne	1.59	1.59	1.56	^{54}Cr	0.59	0.59	0.50
^{24}Mg	0.86	0.86	0.45	^{54}Fe	0.62	0.44	0.44
^{25}Mg	1.14	1.14	0.51	^{56}Fe	0.79	0.45	0.44
^{26}Mg	1.07	1.07	0.66	^{57}Fe	1.04	0.50	0.48
^{28}Si	0.70	0.57	0.44	^{58}Fe	1.29	1.29	0.73
^{29}Si	0.64	0.64	0.46	^{58}Ni	0.71	0.44	0.44
^{30}Si	0.92	0.92	0.47	^{60}Ni	0.91	0.50	0.46
^{32}S	0.71	0.47	0.44	^{61}Ni	1.61	1.07	0.63
^{33}S	0.62	0.56	0.47	^{62}Ni	1.57	0.76	0.54
^{34}S	0.60	0.59	0.45	^{64}Ni	1.37	1.37	0.91
^{36}S	0.75	0.75	0.55	^{64}Zn	0.50	0.45	0.44
^{40}Ca	0.62	0.44	0.44	^{66}Zn	0.72	0.64	0.52
^{42}Ca	0.49	0.49	0.46	^{67}Zn	0.77	0.76	0.56
^{43}Ca	0.60	0.52	0.46	^{68}Zn	0.67	0.67	0.54
^{44}Ca	0.59	0.46	0.45	^{70}Zn	0.57	0.57	0.45
^{46}Ca	0.96	0.96	0.52				

Supplementary Table 4: Core-collapse supernova yields of stable Li, Be, and B isotopes for the 11.8-solar-mass model with no fallback (Case 1)

Isotope	Yield ($M_\odot$)	Case 1	Case 2	Case 3
^{6}Li	1.10(−11)	8.5(−4)	8.5(−4)	8.4(−4)
^{7}Li	1.55(−7)	0.84	0.83	0.82
^{9}Be	5.99(−11)	2.1(−2)	2.1(−2)	2.1(−2)
^{10}B	1.45(−9)	7.6(−2)	7.6(−2)	6.8(−2)
^{11}B	4.25(−7)	5.03	5.00	4.56

Corresponding percentages of the solar system inventories are given for Case 1 and two other cases with fallback. Note that $x(-y)$ denotes $x \times 10^{-y}$.

Supplementary Discussion

Core-collapse supernova (CCSN) yields of stable isotopes. Supplementary Table 2 gives the yields of major stable isotopes for the 11.8 $M_\odot$ CCSN model assuming no fallback (Case 1). As shown in Fig. 1a of the main text, the yields of stable isotopes increase greatly for CCSNe of 14–30 $M_\odot$. For a stable isotope ^{i}E of element E, the percentage of its solar system (SS) inventory contributed by a CCSN is

$$\eta(^i\mathrm{E}) \sim \frac{fY(^i\mathrm{E})}{X_\odot(^i\mathrm{E})M_\odot} \times 100, \tag{S1}$$

where $Y(^i\mathrm{E})$ is its yield, f is the fraction incorporated into each $M_\odot$ of the protosolar cloud, and $X_\odot(^i\mathrm{E})$ is its solar mass fraction. The CCSN contributions would introduce shifts in $^i\mathrm{E}/^j\mathrm{E}$, the number ratio of isotopes ^{i}E and ^{j}E, for SS materials. The percentage shift for macroscopic samples can be estimated as $\delta(^i\mathrm{E}/^j\mathrm{E}) = 100[(^i\mathrm{E}/^j\mathrm{E})/(^i\mathrm{E}/^j\mathrm{E})_\odot - 1] \sim \eta(^i\mathrm{E}) - \eta(^j\mathrm{E})$, where $(^i\mathrm{E}/^j\mathrm{E})_\odot$ is the SS average. No large shifts at the few percent level have been observed for stable isotopes of e.g., Mg, Si, Ca, Fe, and Ni, and the observed large excess in ^{16}O is most likely unrelated to its nucleosynthetic origin [S3].

Supplementary Table 3 gives $\eta(^i\mathrm{E})$ for Case 1 of the 11.8 $M_\odot$ model without fallback and Cases 2 and 3 with fallback, assuming $f \sim 5 \times 10^{-4}$ for all cases. It can be seen that in all cases the above CCSN contributed $\lesssim 1\%$ of the SS inventory for most of the major stable isotopes, with the highest contribution being 2.72% for ^{18}O. The shifts in $^i\mathrm{E}/^j\mathrm{E}$ due to this CCSN are entirely consistent with meteoritic constraints [S3].

In Cases 2 and 3 of the 11.8 $M_\odot$ model with fallback, the percentage contributions to the heaviest Cr (^{54}Cr), Fe (^{58}Fe), and Ni (^{64}Ni) isotopes are the highest among their respective isotopes (see Supplementary Table 3). This arises because fallback is efficient in destroying the products of explosive nucleosynthesis, but has a smaller effect on the neutron-rich isotopes produced by the slow neutron-capture (s) process during pre-CCSN evolution. Macroscopic samples receiving contributions from the 11.8 $M_\odot$ CCSN would typically show excesses of ^{54}Cr/^{52}Cr, ^{58}Fe/^{56}Fe, and ^{64}Ni/^{58}Ni at levels of $\sim 10^{-3}$, similar to those observed in meteorites. As there are few satisfactory explanations of these excesses [S4], this provides additional circumstantial support for the thesis that a low-mass CCSN with modest fallback triggered SS formation. We note that Ref. [S4] explored a different explanation of these excesses by s-processing in asymptotic-giant-branch (AGB) stars. A

crucial distinction between the above two explanations lie in their associated grains that would carry much larger anomalies. Grains from a low-mass CCSN would show excesses of ^{29}Si/^{28}Si and ^{30}Si/^{28}Si (see especially Case 2 in Supplementary Table 3), but those from AGB stars would not [S4].

CCSN production of short-lived radionuclides (SLRs). Most of the ^{10}Be production occurs in the C and O shells, where the mass fraction of ^{12}C is high but that of ^{4}He is low. A low ^{4}He abundance is crucial in avoiding ^{10}Be destruction via $^{10}\mathrm{Be}(\alpha, n)^{13}\mathrm{C}$. For the same reason, neutrino-induced production of ^{10}Be is self-limiting because spallation of ^{12}C and ^{16}O also produces ^{4}He and protons that can destroy ^{10}Be via $^{10}\mathrm{Be}(p, \alpha)^{7}\mathrm{Li}$. As long as abundances of ^{4}He and protons are low, most of the ^{10}Be survives even when the production zone is heated by shock passage. We note that Ref. [S5] adopted a rate for $^{10}\mathrm{Be}(\alpha, n)^{13}\mathrm{C}$ that is orders of magnitude larger than currently recommended [S6], and therefore, greatly underestimated the ^{10}Be yield. In addition, the $16.2\,M_{\odot}$ model used in that work was evolved from a helium core with a fitted hydrogen envelope [S7] while each of our models has been evolved self-consistently as a whole star. We find that the radii of the C/O shell in that $16.2\,M_{\odot}$ model are ~ 2 times larger than those in our $16\,M_{\odot}$ model. Consequently, the neutrino flux for ^{10}Be production was significantly smaller in Ref. [S5], which also contributed to the much smaller yield reported there.

The SLR ^{36}Cl can be produced by neutrinos via $^{36}\mathrm{Ar}(\bar{\nu}_e, e^+)^{36}\mathrm{Cl}$, where the ^{36}Ar is made during shock passage by explosive nucleosynthesis. This channel accounts for $\sim 60\%$ of the ^{36}Cl yield in our $11.8\,M_{\odot}$ model. A significant fraction (up to $\sim 40\%$) of ^{26}Al is made by explosive nucleosynthesis via $^{25}\mathrm{Mg}(p, \gamma)^{26}\mathrm{Al}$, including some enhancement by the protons released from neutrino spallation. ^{53}Mn is almost entirely a product of explosive nucleosynthesis in all of our models.

SLRs are also produced during pre-CCSN evolution: ^{26}Al through hydrostatic burning at the edge of the He shell; ^{36}Cl, ^{41}Ca, ^{107}Pd, and ^{205}Pb mainly through the *s* process associated with He core burning; and ^{60}Fe, ^{135}Cs, and ^{182}Hf mostly through the *s* process associated with C burning in the O shell. The neutrons for the *s* process come from $^{22}\mathrm{Ne}(\alpha, n)^{25}\mathrm{Mg}$, while the seeds come from the progenitor's initial composition, which is taken as solar in all of our models.

For the $11.8\,M_{\odot}$ model with no fallback (Case 1), Supplementary Fig. 1 shows the fraction

of the total yield of each SLR enclosed within a specific radius, as a function of the stellar mass enclosed within the same radius. The left (right) vertical line indicates the boundary between fallback and ejected material for Case 2 (3) with only 1.5% of the innermost $1.02 \times 10^{-2}\,M_\odot$ ($0.116\,M_\odot$) of shocked material ejected. As the enclosed fraction of the ^{10}Be yield sharply increases near the boundary for Case 3, this case represents the limit of reducing ^{53}Mn and ^{60}Fe without affecting the concordance among ^{10}Be, ^{41}Ca, and ^{107}Pd shown in Fig. 2 of the main text.

Reference [S1] used high-mass CCSN models with fallback to explain the meteoritic data on the SLRs ^{26}Al, ^{41}Ca, ^{53}Mn, and ^{60}Fe. Supplementary Table 1 gives the results for our $20\,M_\odot$ and $30\,M_\odot$ models based on similar scenarios. For the $20\,M_\odot$ ($30\,M_\odot$) model, we have used $f \sim 1.1 \times 10^{-3}$ (6.7×10^{-4}) and $\Delta \sim 1.2$ Myr (1.1 Myr) in equation (1) of the main text and assumed that a fraction $q \sim 5 \times 10^{-4}$ (8×10^{-4}) of the shocked material below the fallback boundary at the mass cut $M_{\rm cut} \sim 4.68\,M_\odot$ ($9.38\,M_\odot$) is ejected. The corresponding parameters in Ref. [S1] are $f \sim 1.9 \times 10^{-3}$ (4.35×10^{-4}), $\Delta \sim 1.07$ Myr (0.87 Myr), $q \sim 10^{-3}$ (10^{-3}), and $M_{\rm cut} \sim 3.1\,M_\odot$ ($6.7\,M_\odot$). For our $20\,M_\odot$ ($30\,M_\odot$) model, contributions to the SS inventory of ^{16}O, ^{17}O, and ^{18}O are $\sim 3.1\%$, 1.7%, and 21.6% (0.3%, 0.4%, and 18.1%), respectively. These would have caused large shifts in ^{18}O/^{16}O and ^{17}O/^{18}O that are not observed [S8]. Further, both our models overproduce ^{107}Pd (see Supplementary Table 1 and Table 1 of the main text). No calculation was presented for this SLR in Ref. [S1].

With similar yields of ^{10}Be for CCSNe of 11.8–30 $M_\odot$, production by these sources against decay may maintain an inventory of ^{10}Be in the interstellar medium (ISM). An upper limit on the corresponding mass fraction can be estimated as

$$X_{\rm ISM}(^{10}{\rm Be}) \sim \frac{\langle Y(^{10}{\rm Be})\rangle R_{\rm SN}}{M_{\rm ISM}} \tau(^{10}{\rm Be}) \sim 10^{-14}, \qquad \text{(S2)}$$

where $\langle Y(^{10}{\rm Be})\rangle \sim 5 \times 10^{-10}\,M_\odot$ is the average yield (see Table 1 and Fig. 1b of the main text), $\tau(^{10}{\rm Be}) \sim 2$ Myr is the lifetime, and $R_{\rm SN} \sim (10\ {\rm yr})^{-1}$, the rate of CCSNe in a total mass $M_{\rm ISM} \sim 10^{10}\,M_\odot$ of ISM, is taken near the upper bound of plausible rates. The above estimate can be combined with the mass fraction of ^{9}Be in the ISM, $X_\odot(^9{\rm Be}) \sim 1.4 \times 10^{-10}$, to give $(^{10}{\rm Be}/^9{\rm Be})_{\rm ISM} \sim 6 \times 10^{-5}$ at the time of SS formation. This is ~ 10 times less than the typical value in the early SS (see Table 1 of the main text). As we have shown, the latter can be explained by a low-mass CCSN similar to our $11.8\,M_\odot$ model that triggered the formation of the SS.

CCSN remnant evolution and SLRs in the early SS. The triggering of SS formation and the injection of SLRs into the early SS by a low-mass CCSN depend on the evolution of its remnant. This evolution most likely occurred in a giant molecular cloud with gas of varying density surrounding much denser clumps. The protosolar cloud resided in the core of one of these clumps. For triggering the collapse of the protosolar cloud, the shock velocity associated with remnant expansion should have been $v_{\rm s} \sim 20$–40 km s^{-1} [S9–S11]. There is also a requirement on the remnant size so that a fraction $f \sim 5 \times 10^{-4}$ of the CCSN ejecta was incorporated into each $M_\odot$ of the protosolar cloud to account for the SLRs ^{10}Be, ^{41}Ca, and ^{107}Pd simultaneously. For a remnant with a shock radius $R_{\rm s}$ colliding with a cloud of radius $r_{\rm c}$, only a fraction $\sim r_{\rm c}^2/(4R_{\rm s}^2)$ of the remnant material would be available for injection. So f can be estimated as

$$f \sim \epsilon_{\rm in} \left(\frac{r_{\rm c}^2}{4R_{\rm s}^2}\right) \sim 2.5 \times 10^{-4} \left(\frac{\epsilon_{\rm in}}{0.1}\right) \left(\frac{r_{\rm c}}{0.1 \text{ pc}}\right)^2 \left(\frac{\text{pc}}{R_{\rm s}}\right)^2, \tag{S3}$$

where $\epsilon_{\rm in}$ is the efficiency of injecting the relevant part of the remnant material into each $M_\odot$ of the protosolar cloud. Guided by simulations [S9–S11], we take $\epsilon_{\rm in} \sim 0.1$ for a typical clump core of $\sim 1\, M_\odot$ with $r_{\rm c} \sim 0.1$ pc [S12]. Based on the above discussion, our proposed trigger scenario requires that the low-mass CCSN remnant must have had $v_{\rm s} \sim 20$–40 km s^{-1} and $R_{\rm s} \sim 1$ pc when colliding with the protosolar cloud. In addition, these conditions must have been reached within $\Delta \sim 1$ Myr to account for the pertinent SLRs, especially ^{41}Ca with a very short lifetime of ~ 0.15 Myr.

The shock velocities of concern typically occur when the remnant is in the pressure-driven snowplow (PDS) phase. For reference, we consider the simple case of a CCSN remnant expanding in a uniform ISM. At the onset of the PDS phase, the shock radius $R_{\rm PDS}$ and velocity $v_{\rm PDS}$ [S13] are approximately given by

$$R_{\rm PDS} \sim 1.01 \left(\frac{E}{10^{50} \text{ erg}}\right)^{2/7} \left(\frac{100 \text{ cm}^{-3}}{n_0}\right)^{3/7} \text{ pc}, \tag{S4}$$

$$v_{\rm PDS} \sim 676 \left(\frac{E}{10^{50} \text{ erg}}\right)^{1/14} \left(\frac{n_0}{100 \text{ cm}^{-3}}\right)^{1/7} \text{ km s}^{-1}, \tag{S5}$$

where E is the explosion energy of the CCSN, and n_0 is the number density of hydrogen atoms in the ISM. The remnant evolution during the PDS phase [S13] is approximately

described by

$$R_{\rm s} \sim R_{\rm PDS}\left(\frac{4}{3}t_* - \frac{1}{3}\right)^{3/10}, \tag{S6}$$

$$v_{\rm s} \sim v_{\rm PDS}\left(\frac{4}{3}t_* - \frac{1}{3}\right)^{-7/10}, \tag{S7}$$

where $t_* \equiv t/t_{\rm PDS}$ is the time t since the explosion in units of

$$t_{\rm PDS} \sim 584\left(\frac{E}{10^{50}\ {\rm erg}}\right)^{3/14}\left(\frac{100\ {\rm cm^{-3}}}{n_0}\right)^{4/7}\ {\rm yr}. \tag{S8}$$

Using $E \sim 10^{50}$ erg for the low-mass CCSN and $n_0 \sim 100$ cm^{-3} for a typical giant molecular cloud [S12], we find that for the above simple case, the remnant reaches $v_{\rm s} \sim 40$ km s^{-1} at $t \sim 2.5 \times 10^4$ yr. The corresponding $R_{\rm s} \sim 3.4$ pc gives $f \sim 2 \times 10^{-5}$. This should be regarded as a lower limit on f because the shock wave can be slowed down more efficiently in a giant molecular cloud with dense clumps . For example, if at the onset of the PDS phase the remnant in the simple case encounters a clump with a hydrogen density of $n_0' \sim 2 \times 10^3$ cm^{-3} and a radius of ~ 1 pc [S12], then by momentum conservation relevant for the PDS phase, the shock wave approaches the core of the clump with $v_{\rm s} \sim (n_0/n_0')v_{\rm PDS} \sim 34$ km s^{-1} but its effective radius remains close to $R_{\rm s} \sim 1$ pc. In this example, the conditions for triggering the collapse of the core and injecting SLRs into it would be satisfied. Based on the above discussion, we consider our trigger scenario reasonable and urge that simulations of remnant evolution in a giant molecular cloud be carried out to provide more rigorous results. We note that the time of remnant expansion must have been far shorter than $\Delta \sim 1$ Myr. Therefore, this interval must reflect the timescales associated with the collapse of the protosolar cloud and the formation of the first solids in the early SS.

Evolution of a CCSN remnant prior to the PDS phase is associated with acceleration of cosmic rays (CRs), which can produce ^{10}Be [S14]. We consider the amount of ^{10}Be produced by CRs inside the remnant up to the onset of the PDS phase and compare this to the low-mass CCSN yield. Using $n_0 \sim 100$ cm^{-3} but an explosion energy 10 times too high for the low-mass CCSN, Ref. [S14] found that CRs can produce $^{10}{\rm Be}/^{9}{\rm Be} \sim 2.5 \times 10^{-3}$ at the maximum. Adopting this upper limit and a total mass of swept-up ISM

$$M_{\rm PDS} \sim 10\,M_\odot\left(\frac{n_0}{100\ {\rm cm^{-3}}}\right)\left(\frac{R_{\rm PDS}}{\rm pc}\right)^3, \tag{S9}$$

we estimate that CRs can produce at most $\sim 4 \times 10^{-12}\,M_\odot$ of ^{10}Be, which is far below the low-mass CCSN yield of $\sim 3.26 \times 10^{-10}\,M_\odot$ (see Table 1 of the main text). Therefore, even

allowing for complications of remnant evolution, CR production inside the remnant would have been a subdominant contribution to the ^{10}Be in the early SS.

Reference [S14] considered a remnant interacting with the protosolar cloud and suggested that CR production of ^{10}Be inside the cloud might have provided this SLR to the calcium-aluminum-rich inclusions with Fractionation and Unidentified Nuclear isotope effects (FUN-CAIs). However, it is not clear how this production actually took place when the very small size of the cloud relative to the remnant is taken into account. It is highly desirable to extend the study in Ref. [S14] to our proposed low-mass CCSN trigger scenario.

Potential tests for a low-mass CCSN trigger: Li, Be, B. In our proposed scenario, a low-mass CCSN trigger provided the bulk of the ^{10}Be inventory in the early SS as indicated by canonical CAIs. CR production associated with the CCSN remnant might have provided ^{10}Be to FUN-CAIs [S14]. Any ^{10}Be production by CRs and solar energetic particles (SEPs) [S15, S16] would be in addition to the injection from the CCSN but generally at subdominant levels consistent with the observed variations of ^{10}Be/^{9}Be in canonical CAIs [S17–S20].

We propose a potential test of the above scenario based on the distinct yield pattern of Li, Be, and B isotopes for the CCSN. Supplementary Table 4 gives the yields of ^{6}Li, ^{7}Li, ^{9}Be, ^{10}B, and ^{11}B for the 11.8 $M_{\odot}$ model with no fallback (Case 1). The fallback in Cases 2 and 3 causes little change in these results. It can be seen that the CCSN predominantly produces ^{7}Li and ^{11}B, which is a feature of neutrino-induced nucleosynthesis [S21]. This is in sharp contrast to the production by CRs or SEPs with much higher energy than CCSN neutrinos. For example, Ref. [S14] gave relative number yields of ^{6}Li : ^{7}Li : ^{9}Be : ^{10}B : ^{11}B $\sim$ 1 : 1.8 : 0.11 : 0.43 : 1.1.

The presence of ^{10}Be in the early SS is established by the correlation between ^{10}B/^{11}B and ^{9}Be/^{11}B, from which the initial values $(^{10}\mathrm{Be}/^{9}\mathrm{Be})_0$ and $(^{10}\mathrm{B}/^{11}\mathrm{B})_0$ at the time of ^{10}Be incorporation are obtained. In our scenario, the low-mass CCSN trigger provided the bulk of the ^{10}Be and $\sim$ 5% of the ^{11}B in the SS (see Supplementary Table 4). Consequently, we expect that samples with higher $(^{10}\mathrm{Be}/^{9}\mathrm{Be})_0$ would have lower $(^{10}\mathrm{B}/^{11}\mathrm{B})_0$ due to the excess of ^{11}B over ^{10}B that accompanied the ^{10}Be from the CCSN. The variations in $(^{10}\mathrm{B}/^{11}\mathrm{B})_0$ should be at the level of $\sim$ 5%. Such variations are consistent with the data reported in Refs. [S19, S20]. It remains to be seen if future meteoritic studies with more samples and better precision can establish the above relationship rigorously, thereby providing a test for the low-mass CCSN trigger.

A correlation between ^{7}Li/^{6}Li and ^{9}Be/^{6}Li was found in a sample with $(^{10}\mathrm{Be}/^{9}\mathrm{Be})_0 = (8.8 \pm 0.6) \times 10^{-4}$ and interpreted as indicating the presence of the SLR ^{7}Be in the early SS [S22]. If true, the extremely short lifetime of 77 days for ^{7}Be would almost certainly require irradiation by SEPs for its production, and by association, the same mechanism may also have produced the ^{10}Be in the sample. However, the above result was disputed and the controversy remains unresolved [S23, S24]. Here we propose an alternative explanation for the tantalizing correlation between ^{7}Li/^{6}Li and ^{9}Be/^{6}Li. We note that the low-mass CCSN trigger also provided $\sim 0.8\%$ of the ^{7}Li in the SS but a negligible amount of ^{6}Li. We expect that portions of a sample that received higher amounts of ^{10}Be from the CCSN would also have higher amounts of ^{7}Li. For a uniform $(^{10}\mathrm{Be}/^{9}\mathrm{Be})_0$ across the sample, the above relationship would translate into an apparent correlation between ^{7}Li/^{6}Li and ^{9}Be/^{6}Li, which nevertheless has nothing to do with the presence of ^{7}Be in the early SS. This explanation can be tested more directly by checking the relationship between ^{7}Li/^{6}Li and $(^{10}\mathrm{Be}/^{9}\mathrm{Be})_0$ for a wide range of samples. In our scenario, ^{7}Li/^{6}Li should increase with $(^{10}\mathrm{Be}/^{9}\mathrm{Be})_0$. As only a relatively small amount of ^{7}Li was added by the low-mass CCSN, high-precision measurements are required to check this relationship. Such measurements would provide an additional test for the low-mass CCSN trigger and also help resolve the controversy over the ^{7}Be result.

Supplementary References

[S1] Takigawa, A. *et al.* Injection of short-lived radionuclides into the early solar system from a faint supernova with mixing fallback. *Astrophys. J.* **688**, 1382–1387 (2008).

[S2] Takahashi, K. & Yokoi, K. Beta-decay rates of highly ionized heavy atoms in stellar interiors. *At. Data Nucl. Data Tables* **36**, 375–409 (1987).

[S3] Wasserburg, G. J., Busso, M., Gallino, R. & Nollett, K. M. Short-lived nuclei in the early solar system: Possible AGB sources. *Nucl. Phys. A* **777**, 5–69 (2006).

[S4] Wasserburg, G. J., Trippella, O. & Busso, M. Isotope anomalies in the Fe-group elements in meteorites and connections to nucleosynthesis in AGB stars. *Astrophys. J.* **805**, 7 (2015).

[S5] Yoshida, T. *et al.* Neutrino-nucleus reaction cross sections for light element synthesis in supernova explosions. *Astrophys. J.* **686**, 448–466 (2008).

[S6] Cyburt, R. H. *et al.* The JINA REACLIB database: Its recent updates and impact on type-I X-ray bursts. *Astrophys. J. Suppl. Ser.* **189**, 240–252 (2010).

[S7] Shigeyama, T. & Nomoto, K. Theoretical light curve of SN 1987A and mixing of hydrogen and nickel in the ejecta. *Astrophy. J.* **360**, 242–256 (1990).

[S8] Clayton, R. N., Grossman, L. & Mayeda, T. K. A component of primitive nuclear composition in carbonaceous meteorites. *Science* **182**, 485–488 (1973).

[S9] Boss, A. P. & Keiser, S. A. Who pulled the trigger: A supernova or an asymptotic giant branch star? *Astrophy. J.* **717**, L1–L5 (2010).

[S10] Boss, A. P. & Keiser, S. A. Triggering collapse of the presolar dense cloud core and injecting short-lived radioisotopes with a shock wave. III. Rotating three-dimensional cloud cores. *Astrophys. J.* **788**, 20 (2014).

[S11] Boss, A. P. & Keiser, S. A. Triggering collapse of the presolar dense cloud core and injecting short-lived radioisotopes with a shock wave. IV. Effects of rotational axis orientation. *Astrophys. J.* **809**, 103 (2015).

[S12] Bergin, E. A. & Tafalla, M. Cold dark clouds: The initial conditions for star formation. *Annu. Rev. Astron. Astrophys.* **45**, 339–396 (2007).

[S13] Cioffi, D. F., McKee, C. F. & Bertschinger, E. Dynamics of radiative supernova remnants. *Astrophys. J.* **334**, 252–265 (1988).

[S14] Tatischeff, V., Duprat, J. & de Séréville, N. Light-element nucleosynthesis in a molecular

cloud interacting with a supernova remnant and the origin of beryllium-10 in the protosolar nebula. *Astrophys. J.* **796**, 124 (2014).

[S15] Gounelle, M. *et al.* Extinct radioactivities and protosolar cosmic rays: Self-shielding and light elements. *Astrophys. J.* **548**, 1051–1070 (2001).

[S16] Gounelle, M. *et al.* The irradiation origin of beryllium radioisotopes and other short-lived radionuclides. *Astrophys. J.* **640**, 1163–1170 (2006).

[S17] McKeegan, K. D., Chaussidon, M. & Robert, F. Incorporation of short-lived ^{10}Be in a calcium-aluminum-rich inclusion from the Allende meteorite. *Science* **289**, 1334–1337 (2000).

[S18] MacPherson, G. J., Huss, G. R. & Davis, A. M. Extinct ^{10}Be in Type A calcium-aluminum-rich inclusions from CV chondrites. *Geochim. Cosmochim. Acta* **67**, 3165–3179 (2003).

[S19] Wielandt, D. *et al.* Evidence for multiple sources of ^{10}Be in the early solar system. *Astrophys. J.* **748**, L25 (2012).

[S20] Srinivasan, G. & Chaussidon, M. Constraints on ^{10}Be and ^{41}Ca distribution in the early solar system from ^{26}Al and ^{10}Be studies of Efremovka CAIs. *Earth Planet. Sci. Lett.* **374**, 11–23 (2013).

[S21] Woosley, S. E., Hartmann, D. H., Hoffman, R. D. & Haxton, W. C. The ν-process. *Astrophys. J.* **356**, 272–301 (1990).

[S22] Chaussidon, M., Robert, F. & McKeegan, K. D. Li and B isotopic variations in an Allende CAI: Evidence for the in situ decay of short-lived ^{10}Be and for the possible presence of the short-lived nuclide ^{7}Be in the early solar system. *Geochim. Cosmochim. Acta* **70**, 224–245 (2006).

[S23] Desch, S. J. & Ouellette, N. Comment on "Li and Be isotopic variations in an Allende CAI: Evidence for the in situ decay of short-lived ^{10}Be and for the possible presence of the short-lived nuclide ^{7}Be in the early solar system," by M. Chaussidon, F. Robert, and K.D. McKeegan. *Geochim. Cosmochim. Acta* **70**, 5426–5432 (2006).

[S24] Chaussidon, M., Robert, F. & McKeegan, K. D. Reply to the comment by Desch and Ouellette on "Li and B isotopic variations in an Allende CAI: Evidence for the in situ decay of short-lived ^{10}Be and for the possible presence of the short-lived nuclide ^{7}Be in the early solar system". *Geochim. Cosmochim. Acta* **70**, 5433–5436 (2006).